Tunneling and nonparabolicity effects in in-plane magnetic fields

G. Rainer, J. Smoliner, and E. Gornik
Institut für Festkörperelektronik, Floragasse 7, A-1040 Wien, Austria

G. Böhm and G. Weimann
Walter Schottky Institut, Technische Universität München, D-8046 Garching, Germany
(Received 5 December 1994)

In this paper, tunneling processes between two two-dimensional electron systems in in-plane magnetic fields are used to investigate the nonparabolicity in the GaAs conduction band. The two two-dimensional systems are realized on a GaAs-$Ga_{1-x}Al_xAs$ heterostructure and are separated by a barrier of only 200 Å. All resonant tunneling processes between the quantized states on each side of the barrier are reflected as large and narrow peaks in the current-voltage characteristics. If a small magnetic field is applied perpendicular to the direction of the tunneling current, all resonance peaks are significantly broadened and shifted to different bias voltages. In addition, these peaks exhibit a characteristic shoulder, which is not present at zero magnetic fields. The broadening of the resonances is well understood in terms of common models, but to explain the shifting of the peaks and the formation of the characteristic shoulder, different effective masses in the emitter and collector electrode have to be assumed. Comparing the experimental data with the results of a model calculation, the effective mass in the two-dimensional subbands is determined as a function of energy.

INTRODUCTION

Resonant tunneling experiments with in-plane magnetic fields have been performed on very different structures during the past years. The most common configuration is the double-barrier heterostructure, which consists of two barriers with a quantum well in between. The electrodes on both sides of the structure are of three-dimensional character, whereas the motion of the electrons is completely quantized inside the well, where a two-dimensional electron gas (2DEG) is formed between the barriers. Results on this system have been reported for GaAs-$Al_xGa_{1-x}As$ (Refs. 1–4) and InP-$In_{1-x}Ga_xAs$ (Ref. 5) heterostructures. Similar experiments were carried out on barrier-separated superlattices.[6] For single-barrier structures, the situation becomes very simple for tunneling processes between two sets of states on both sides of the barrier if the dependence of the transmission probability on the electron energy can be neglected. With applied in-plane magnetic fields, the corresponding features in the current-voltage $I(V_b)$ characteristics broaden significantly and shift to higher energies. More recently, attention has been focused on the valence band. In the GaAs-AlAs system,[7] a double-barrier configuration was used to study the subbands in the central quantum well in the valence band, where in this case the emitter was of two-dimensional character. For the Si-SiGe system,[8,9] tunneling in in-plane magnetic fields has been used to study in-plane effective masses of the valence subbands, and angular anisotropy. In contrast to optical measurements, which tend to average over k space, magnetotunneling spectroscopy allows the investigation of specific k values, since both energy and momentum must be conserved for a resonant tunneling process. Thus, only particles eligible for tunneling contribute to the resonant current. The dependence of peak position and the shape of the resonance peak on in-plane magnetic fields yields valuable information on the band structure of the investigated sample.

In a previous paper,[10] we have investigated a 2D-2D tunneling structure, which consists of an inversion layer and an accumulation layer separated by barrier of 200 Å. This structure corresponds to a single-barrier system with quantized 2D states on each side of the barrier. All transitions between the quantized states were evident as large peaks in the dI/dV_b characteristics, which can be used to determine subband spacings or even the residual impurity concentration in the GaAs buffer layer.[11] In small in-plane magnetic fields, the observed resonance peaks were split into two peaks, which were used to verify the canonical momentum conservation and to determine the tunneling distances between the initial and final states.

In this paper, results for the above 2D-2D tunneling structure are reported, which were obtained on samples of much higher quality compared to the samples used in Ref. 10. All resonance structures are now resolved in the $I(V_b)$ curves as a series of several sharp and narrow peaks. For this experiment, the $I(V_b)$ curves were recorded with small in-plane magnetic fields ($B < 1$ T). The resonant features exhibit different behavior as a function of the applied magnetic field, depending on whether both or just the emitter subband or the emitter and the collector subbands are occupied by electrons. In the first case, an increasing magnetic field causes the resonant peak at $B = 0$ T to split into two peaks, which shift to higher and lower energies. When the collector subband is empty, the resonant feature shifts to higher energy, and exhibits a characteristic shoulder. Comparing this

behavior with computer-simulated $I(V_b)$ curves, it is shown that these features are due to a different effective mass in the emitter and collector electrodes.

EXPERIMENT

The samples consist of an unintentionally p-doped GaAs layer grown on a semi-insulating substrate ($N_A < 1\times10^{15}$ cm^{-3}), followed by an undoped spacer ($d=50$ Å), doped $Al_xGa_{1-x}As$ ($d=50$ Å, $N_D=3\times10^{18}$ cm^{-3}, $x=35\%$), another spacer ($d=100$ Å), and n-doped GaAs ($d=800$ Å, $N_D=1.2\times10^{15}$ cm^{-3}). An additional GaAs cap layer was highly n-doped ($d=150$ Å, $N_D=6.2\times10^{18}$ cm^{-3}). Shubnikov–de Haas measurements were used to determine the electron concentrations in the inversion and accumulation layers at liquid-helium temperature ($n^{inv}=6.3\times10^{11}$ cm^{-2}, $n^{acc}=5.7\times10^{11}$ cm^{-2}). The spacer thicknesses were chosen asymmetrically to enhance the electron mobility at the inverted interface of the accumulation layer ($\mu^{acc}=35\,000$ cm^2/V s, $\mu^{inv}=130\,000$ cm^2/V s). A self-consistently calculated conduction-band profile is shown in Fig. 1. E_n^{inv}, E_F^{inv}, E_0^{acc}, and E_F^{acc} denote the subbands and Fermi energies in the inversion and accumulation layers, respectively. n is the subband index. For clarity, the charge-density distributions of some subbands are also shown. Ohmic contacts to the 2D channels were aligned using a AuGe alloy. To establish the tunneling contact, a AuGe film was slightly diffused into the upper GaAs layers. Finally, the GaAs around the top contact was removed selectively, yielding independent contacts to both 2D channels. All series resistances in the lower 2DEG and in the top electrode were compensated by a four-terminal conduction bridge.[12] To measure the derivative of the tunneling, dI/dV_b, a modulation frequency of 22 Hz and a modulation voltage of 0.1 mV were used to avoid parasitic capacitive effects and to achieve a high resolution.

If a voltage is applied to the tunnel junction, the 2D states on both sides of the barrier are shifted in energy with respect to each other, which is also shown in Fig. 1. For all 2D-2D tunneling processes, the conservation of the electron momentum parallel to the barrier is required and therefore structures in the tunneling current are only expected if two subbands on each side of the barrier are aligned in energy.[13]

A typical $I(V_b)$ curve, which was recorded at a temperature of 15 K and magnetic field of 0 T, is shown in Fig. 2. Note that this value of T was only chosen to demonstrate the influence of finite temperatures. A detailed analysis of temperature effects will be published elsewhere. The peaks, which correspond to transitions between the subbands on both sides of the barrier, are marked by arrows. For positive bias voltages, one peak is observed, which corresponds to the transition from the E_0^{inv} to E_0^{acc} subband [(0-0) transition]. The peaks at negative bias voltages are due to transitions from the E_0^{acc} subband to higher, unoccupied bands in the inversion layer [(0-1), (0-2), . . . transitions; subband data are summarized in Table I]. Note that we have demonstrated earlier[10,11] that the relative energy shift of both 2D systems in good approximation is equal to $e\Delta V_b$, which means that the voltage spacing between the resonance peaks is equal to the corresponding subband spacing ($\Delta V=\Delta E/e$). The downward arrows mark the peak positions at $B=0$ T, the upward arrows mark the peak positions at $B=0.3$ T, where the orientation of the magnetic field is perpendicular to the tunneling current. These transverse magnetic fields or so-called in-plane magnetic fields cause a broadening of the resonance structures in the $I(V_b)$ characteristics, because tunneling is now allowed for a broad range of energies and not only for the situation where the 2D subband edges are aligned. Thus, all peaks which correspond to transitions into higher

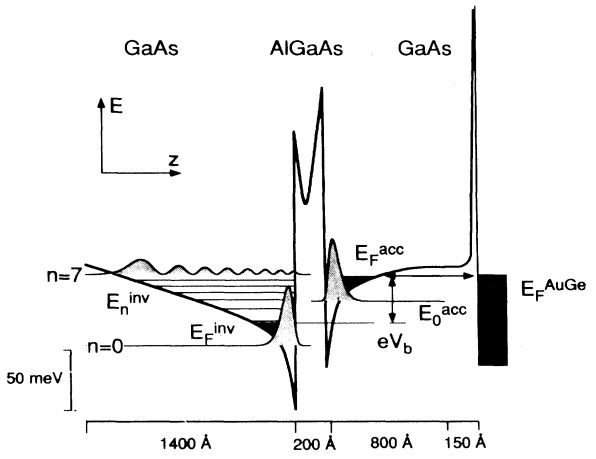

FIG. 1. Schematic view of the conduction-band profile at a bias voltage V_b. E_n^{inv} and E_0^{acc} denote the subband energies in the inversion and accumulation layers. E_F^{inv} and E_F^{acc} are the corresponding Fermi energies. E_F^{AuGe} is the Fermi energy in the top AuGe electrode and V_b is the applied bias voltage.

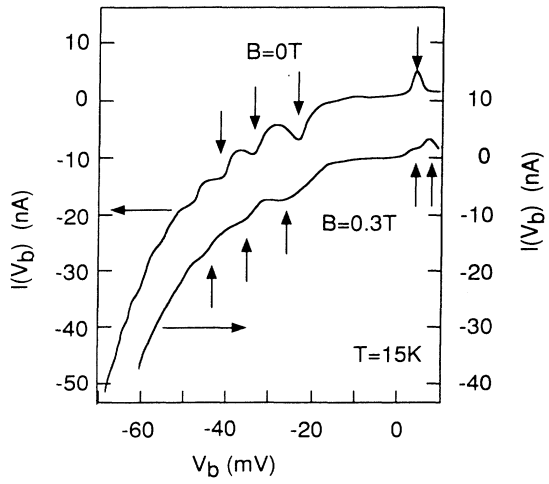

FIG. 2. Two typical $I(V_b)$ curves recorded at $T=15$ K for $B=0$ T (left scale) and $B=0.3$ T (right scale). The arrows mark the resonance-peak positions.

TABLE I. The subband identifiers correspond to the nth subbands in the accumulation and inversion layers. $\langle z \rangle$ is the expectation value of the z coordinate in real space. E_F is the Fermi energy for the inversion and accumulation layers.

Subband	Energy (meV)	$\langle z \rangle$ (Å)	E_F (meV)
acc $n=0$	44.5	74	19.1
inv $n=0$	40.0	63	23.6
inv $n=1$	67.3	145	
inv $n=2$	77.6	216	

unoccupied subbands in the inversion channel shift to higher energies and become asymmetric. In contrast to that, the (0-0) peak splits into two peaks, which are also marked by upward arrows. The main peak shift to higher energies, and in addition, a smaller peak appears, which shifts to lower energies with increasing magnetic fields.

To describe the above effects, we start with tunneling processes at zero magnetic fields. The energy of the electrons in the 2D system is given by

$$E = E_z + \frac{\hbar^2}{2m^*}(k_x^2 + k_y^2) , \tag{1}$$

where k_x and k_y are the transverse momenta, E_z is the subband energy, and m^* is the electron effective mass. Both k_x and k_y may take values from 0 to k_F. Thus, at $T=0$ K the occupied states lie on a paraboloid, which has its vertex at $k_x = k_y = 0$, and they are distributed evenly on the paraboloid, because the density of states of the two-dimensional system is independent of the energy. For finite temperatures, the density of state must be modulated by the Fermi function, to take thermal excitation into account. This yields the following expression:

$$D(\varepsilon) f(\varepsilon, T) = \frac{m^*}{\pi\hbar^2} \frac{1}{e^{(\varepsilon - \varepsilon_F)/k_B T} + 1} . \tag{2}$$

As earlier, one can assume that the parabolic dispersion on both sides is shifted with respect to each other by an amount eV_b when a bias voltage V_b is applied to the structure. Canonical momentum and total energy must be conserved in the resonant tunneling process, which leads to the following selection rules:

$$\begin{aligned} &k_x^{\mathrm{acc}} = k_x^{\mathrm{inv}} , \quad k_y^{\mathrm{acc}} = k_y^{\mathrm{inv}} , \\ &E_z^{\mathrm{acc}} = E_z^{\mathrm{inv}} + eV_b . \end{aligned} \tag{3}$$

Note that total energy

$$E_z + \frac{\hbar^2 k_x^2}{2m^*} + \frac{\hbar^2 k_y^2}{2m^*}$$

is really conserved; however, in the $B=0$ T case, conservation of total energy and conservation of subband energy are equivalent. Only initial states which have unoccupied final states available contribute to the current. Thus, the tunnel current is obtained by integrating over all states of the wave vector $\mathbf{k}$ that satisfy the conservation laws, taking the occupation statistics for initial and final states into account. The effective mass has the same value for both subbands, because they are at a similar distance from the band edge. Thus, tunneling is allowed for just one value of bias voltage, where the paraboloids overlap exactly and the relation $E_0^{\mathrm{acc}} = E_0^{\mathrm{inv}} + eV_b$ is thus sufficient to describe the position of the current maximum. Note that the occupation statistics has an influence on signal strength, because some target states are occupied and do not allow resonant tunneling.

As the next step, the effect of an in-plane magnetic field is considered. The Schrödinger equation is written as

$$\left[\frac{1}{2m^*}(p - eA)^2 + U(r) \right] \psi_k(r) = E_k \psi_k(r) . \tag{4}$$

With the magnetic field in the x direction, the vector potential in the Landau gauge is $A = (0, -Bz, 0)$. This allows a solution of the form $\psi_\nu(r) = e^{ik_x x} e^{ik_y y} \varphi_\nu(z)$. Using first-order perturbation theory, one obtains the following expression for the total energy:

$$E_{\mathrm{tot}} = E_z + \frac{\hbar^2 k_x^2}{2m^*} + \frac{\hbar^2}{2m^*} \left\{ k_y - \frac{\langle z_\nu \rangle}{l^2} \right\}^2 , \tag{5}$$

where $l = \sqrt{\hbar/eB}$ is the magnetic length and $\langle z_\nu \rangle$ is the expectation value of the z coordinate in the νth subband. These expectation values were taken from self-consistent solutions of the Schrödinger and Poisson equations. The magnetic field causes the paraboloid of occupied states to shift its vertex from $k_y = 0$ to $\langle z_\nu \rangle / l^2$, whereas the dispersion relation in the k_x direction is unaffected. The selection rules for resonant tunneling with in-plane magnetic fields are

$$\begin{aligned} &k_x^{\mathrm{acc}} = k_x^{\mathrm{inv}} , \\ &\left[k_y^{\mathrm{acc}} - \frac{\langle z_\nu^{\mathrm{acc}} \rangle}{l^2} \right] = \left[k_y^{\mathrm{inv}} - \frac{\langle z_\nu^{\mathrm{inv}} \rangle}{l^2} \right] , \\ &E_{\mathrm{tot}}^{\mathrm{acc}} = E_{\mathrm{tot}}^{\mathrm{inv}} + eV_b . \end{aligned} \tag{6}$$

For a particular transition, the states eligible for tunneling are represented by the intersection of the two paraboloids. As in the 0-T case, an applied bias voltage shifts the paraboloids with respect to each other. The tunneling probability does not vary strongly with energy, because the barrier height is much larger than the applied bias voltages. The tunneling current is directly proportional to the number of states for which tunneling is allowed by the conservation laws.

To analyze the experimental data quantitatively, the number of tunneling states were calculated as a function of bias voltage, magnetic field, and temperature. For all values of $\mathbf{k} = (k_x, k_y)$ where tunneling is allowed, the expression for the differential current $\Delta j = \{ f_L(\mathbf{k}) - f_R(\mathbf{k}) \} \Delta k^2$ was evaluated, where f_L and f_R represent the distribution functions on the left and right sides of the barrier. Integration over all relevant k values yields the total tunneling current at that bias voltage. It must be pointed out that in contrast to the 0-T case, it is nontrivial to predict the peak position in the tunneling

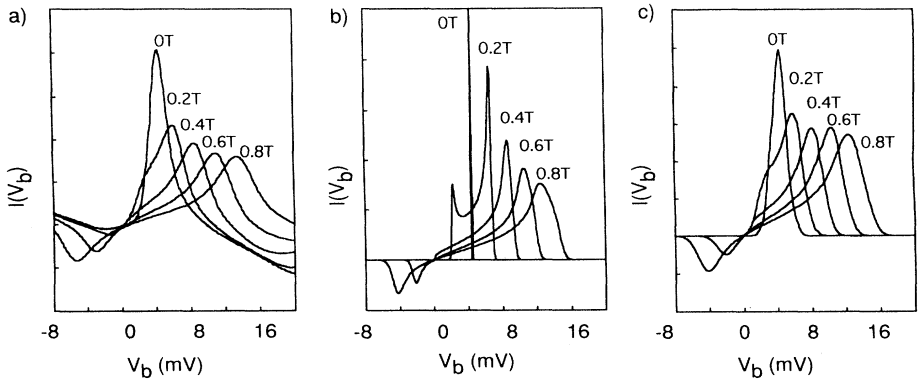

FIG. 3. (a) Experimental $I(V_b)$ curve of the (0-0) transition for five values of B. (b) Simulated results for (0-0) transition. (c) Convolution of simulated $I(V_b)$ curve with Gaussian function.

current with applied magnetic field, because the peak corresponds to that value of bias voltage where the largest number of states are allowed to tunnel. Where this value lies is not immediately obvious. Apart from the position of the peak, the calculation yields the shape of the resonant structures, and thus allows detailed comparisons with experimental data.

First, the results for the (0-0) transition are discussed. Figure 3(a) shows a measured curve, recorded at $T=15$ K for several magnetic fields. Note that the experimentally obtained curves contain an exponential background of nonresonant current (see Fig. 2), which has been subtracted here to obtain the pure resonant signal. The corresponding calculated curves are shown in Fig. 3(b). For both subbands, a constant effective mass of 0.067 was used. The 0-T peak in the simulated curve resembles a δ-like peak, whereas the experimental peak has a linewidth of about 2.5 mV. This broadening is attributed to imperfections of the sample, and is not a temperature effect. With increasing magnetic field, a clear splitting of the 0-T peak is observed both for the calculated and measured curves. For better understanding, one can momentarily neglect the k_x direction, which is not affected by the magnetic field. The k_y selection rules are then represented by two parabolas, each filled to the corresponding Fermi energy, and shifted with respect to each other by a bias voltage V_b. The situation for a small magnetic field is shown in Figs. 4(a)–4(c). In Figs. 4(a) and 4(c), all electrons are allowed to tunnel from the accumulation into the inversion layer or vice versa. In Fig. 4(b) it is clear that only a small number of electrons can tunnel from the accumulation layer into the inversion layer, because most of the final states in the inversion layer are occupied. Thus, a forbidden region of k values appears, where the corresponding current is zero. At $V_b=0$, tunneling ceases, because the system is in equilibrium. At larger magnetic fields—here, for $B>0.5$ T—a situation arises where occupied states in the accumulation layer overlap with empty states of the inversion layer. A negative peak appears at negative bias voltages, which corresponds to tunneling into the inversion layer and is also present in the measured curve. However, this peak is always smaller than the one at positive bias voltages. In Fig. 3(c), the simulated curve was convoluted with an appropriate Gaussian function, to take sample imperfections into account. As the resulting set of curves is in very good agreement with experiment, one can conclude that the model is very adequate, at least for small magnetic fields. In particular, the assumption of a locally parabolic and isotropic effective mass is justified in this

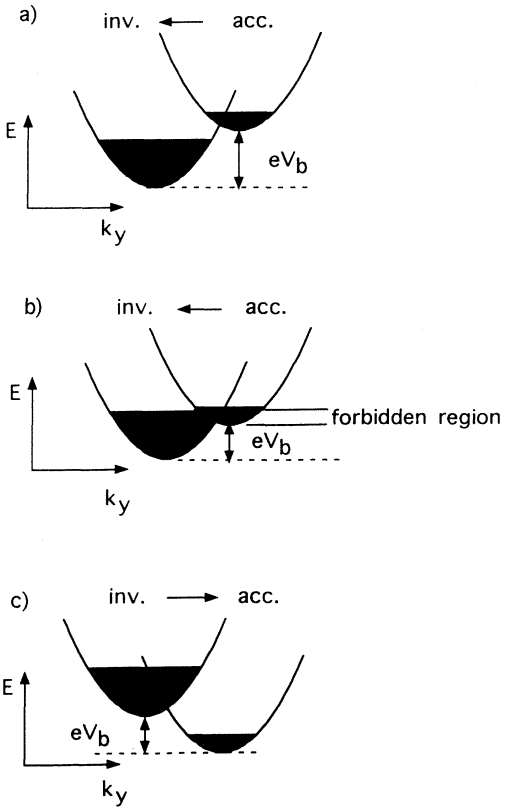

FIG. 4. Graphical representation of the tunneling selection rules for the (0-0) transition. The parabolas represent the dispersion relations of the subbands involved; each is filled to the respective Fermi energy. In (a) and (c) tunneling is allowed and possible, because initial states are filled and the target states are empty. (b) shows the forbidden tunneling region, since all target states are occupied in this regime.

case.

Now the results for the transitions into empty subbands of the inversion layer are considered. All of these are similar, so it suffices to treat one such transition. The (0-1) tunneling process was chosen, because the background of the nonresonant current is smaller than in the other cases, and it exhibits the largest peak-to-valley ratio. The experimental curve is shown in Fig. 5(a). The 0-T peak is broader than the corresponding peak in the (0-0) transition, with a linewidth of about 5 mV. With increasing magnetic field, the peaks shift to higher voltages and display a characteristic "shoulder." This effect is not due to occupied target states, as is the case for the (0-0) transition, since the target subband here is completely empty. It is shown below that this peak shift can be explained by nonparabolicity effects.

Figure 5(b) shows the calculated curves for this transition, on the assumption that the effective mass is constant and equal to 0.067 for both accumulation and inversion layers. Clearly, the peaks do not shift, and only resonance broadening takes place. Furthermore, the 0-T peak, after appropriate convolution, has a linewidth comparable to that of the corresponding peak for the (0-0) transition, which does not agree with experiment. However, postulating a higher effective mass for the inversion layer yields results that are in good agreement with experiment. The assumption is justified, because the target subband has a larger subband energy, and consequently lies further away from the band edge. If the effective mass of the accumulation layer is assumed to be $m_{\rm eff}^{\rm acc,0}=0.0670$, an inversion layer effective mass of $m_{\rm eff}^{\rm inv,1}=0.0696$ yields the best results, which are shown in Fig. 5(b), and after convolution in Fig. 5(c). The 0-T peak of the simulated curve is not δ-like, as in the (0-0) transition, but exhibits a plateau. This accounts for the increased linewidth in the (0-1) case. With increasing magnetic field, the peaks shift towards higher energies, and exhibit the characteristic shoulder which is also present in the experimental curve. Note that the agreement between experimental and simulated curves is good for low magnetic fields only, because the Fermi energy of the accumulation layer has the same order of magnitude as the subband separation. Thus, the assumption of local parabolicity is valid only for small magnetic fields, where the behavior is dominated by states near $k_x=k_y=0$. The effective mass can also be obtained by cyclotron resonance (CR) experiments,[14] where the effective mass of electrons near the Fermi energy is measured. Values of $m_{\rm eff}^{\rm CR}$ obtained in this way are also larger than the band-edge effective masses, and are thus consistent with our results.

In Fig. 6 the effective mass is plotted as a function of the energy offset with respect to the lowest subband in the inversion layer. For the (0-0) transition, the effective masses were assumed equal for both the accumulation and the inversion layers. Comparisons between experimental and calculated curves for the (0-1) and (0-2) transitions were used to determine the average effective masses in the corresponding subbands. As one can see, the mass first increases linearly, but then the curve bends and the effective mass depends less on the increasing energy. Qualitatively, this behavior is understood by the following arguments: For low subband indices, the elec-

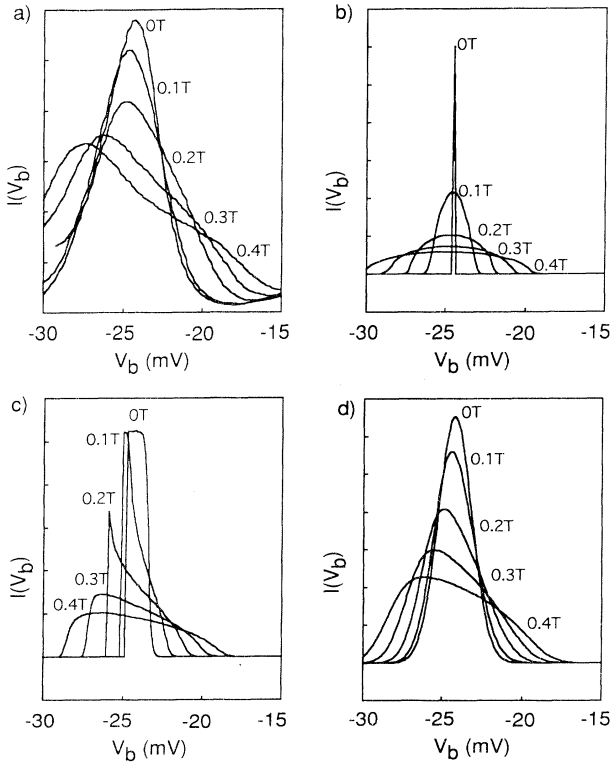

FIG. 5. (a) Measured $I(V_b)$ curve around the (0-1) peak position for five values of B. (b) Corresponding simulated $I(V_b)$ curve with $m_{\rm eff}^{\rm acc}=0.067$ and $m_{\rm eff}^{\rm inv}=0.067$. (c) Corresponding simulated $I(V_b)$ curve with $m_{\rm eff}^{\rm acc}=0.0670$ and $m_{\rm eff}^{\rm inv}=0.0696$. (d) Convolution of simulated curve (c) with appropriate Gaussian function.

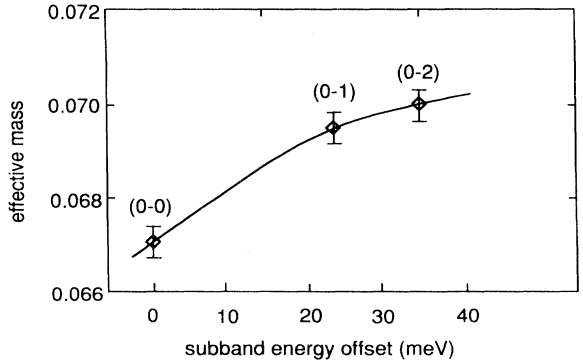

FIG. 6. Effective mass as a function of the energy offset with respect to the lowest subband in the inversion layer. The error bars indicate the experimental error. The solid curve is a guide to the eye.

tron is confined close at the GaAs-$Al_xGa_{1-x}As$ interface, which means that the whole wave function is high above the GaAs band edge. For high subband indices, however, the wave function is extended deeper into the GaAs in our almost triangular potential. This means that for the higher subbands, a major part of the wave function is closer to the GaAs band edge than a wave function of a lower subband, which is located directly at the GaAs-$Al_xGa_{1-x}As$ interface (see Fig. 1). Thus, the effective mass is expected to increase more slowly with increasing energy, which is consistent with the observed behavior.

It must be pointed out that the resolution of our method is very high. Relative changes in the effective mass below 1% are easily resolved, which is comparable or even better than the resolution obtained in far-infrared measurements. This accuracy can be improved, especially for higher energies, if a sample with higher peak-to-valley ratios for resonant transitions into the higher 2D subbands is used. There are mainly two further ways to enhance the experimental accuracy. One is to decrease the electron concentration n_{acc}, which leads to a decreased Fermi energy E_F^{acc} and reduces the averaging over the finite $k_{\parallel}$ range between $k=0$ and $k=k_f$. Second, one could use one-dimensional emitter electrodes in the accumulation layer, which means that almost all electrons are located in a small energy range close to the 1D subband edge. These two methods result in a smaller range of effective masses present in the emitter electrode and the postulation of a locally constant effective mass for each subband would be fulfilled more accurately. In addition, a back-gate voltage can be applied to modify the subband energies and electron densities in the 2D systems. Tuning the subband energies in the inversion layer and measuring the peak positions and amplitudes as a function of the magnetic field, it is then possible to determine the effective mass over a continuous energy range and not only at certain energy values as in the present experiment.

Note, that the above data can also be used to determine tunneling distances in transverse magnetic fields.[10] However, as the resonances are now evident in the $I(V_b)$ curves directly, the width of the $I(V_b)$ peaks determines the resonant tunneling regime between $k=0$ and $k=k_f$. Thus, the widths of the $I(V_b)$ peaks have to be used to determine the tunneling distances instead of the split dI/dV_b peak positions, as in our earlier work.

SUMMARY

In summary, we have investigated tunneling processes between two 2D systems in in-plane magnetic fields. Small magnetic fields, which are applied perpendicular to the direction of the tunneling current, cause a significant broadening of the resonance peaks. The broadening of the resonance peaks is explained by the magnetic-field-induced broadening of the resonant tunneling regime, which is due to a relative shift of the dispersion relations of the emitter and collector states in k space. The shift of the resonance peaks and the characteristic shoulder, however, are only explained if different effective masses in the 2D emitter and collector electrodes are assumed. A comparison with model calculations shows that these effects are extremely sensitive to the difference of the effective mass in the emitter and collector electrodes, which allows a high-resolution probing of the nonparabolicity in the GaAs conduction band.

ACKNOWLEDGMENT

This work was sponsored by Oesterreichische Nationalbank, Project No. 4874.

[1]E. E. Mendez, L. Esaki, and W. I. Wang, Phys. Rev. B **33**, 2893 (1986).
[2]J. A. Lebens, H. H. Silsbee, and S. L. Wright, Phys. Rev. B **37**, 10 308 (1988).
[3]S. Ben Amor, K. P. Martin, J. J. L. Rascol, R. J. Higgins, A. Torabi, H. M. Harris, and C. J. Summers, Appl. Phys. Lett. **53**, 2540 (1988).
[4]P. Gueret, A. Baratoff, and E. Marclay, Europhys. Lett. **3**, 367 (1987).
[5]M. L. Leadbetter, L. Eaves, P. E. Simmonds, G. A. Toombs, F. W. Sheard, P. A. Claxton, G. Hill, and M. A. Pate, Solid State Electron. **31**, 707 (1988).
[6]R. A. Davies, D. J. Newson, T. G. Powell, M. J. Kelly, and H. W. Myron, Semicond. Sci. Technol. **2**, 61 (1987).
[7]R. K. Hayden, D. K. Maude, L. Eaves, E. C. Valdares, M. Henini, F. W. Sheard, O. H. Hughes, J. C. Portal, and L. Cury, Phys. Rev. Lett. **66**, 1749 (1991).
[8]V. P. Kesan, U. Gennser, D. A. Syphers, T. P. Smith, and S. S. Iyer, J. Vac. Sci. Technol. B **11**, 1140 (1993).
[9]G. Schuberth, G. Abstreiter, E. Gornik, E. Schäffler, and J. F. Luy, Phys. Rev. B **43**, 2280 (1991).
[10]J. Smoliner, W. Demmerle, G. Berthold, E. Gornik, G. Weimann, and W. Schlapp, Phys. Rev. Lett. **63**, 2116 (1989).
[11]N. Reinacher, W. Demmerle, J. Smoliner, E. Gornik, G. Weimann, and G. Böhm, J. Appl. Phys. **74**, 3593 (1993).
[12]R. Christanell and J. Smoliner, Rev. Sci. Instrum. **59**, 1290 (1988).
[13]W. Demmerle, J. Smoliner, G. Berthold, E. Gornik, G. Weimann, and W. Schlapp, Phys. Rev. B **44**, 3090 (1991).
[14]C. T. Liu, S. Y. Lin, D. C. Tsui, H. Lee, and D. Ackley, Appl. Phys. Lett. **53**, 25 (1988).

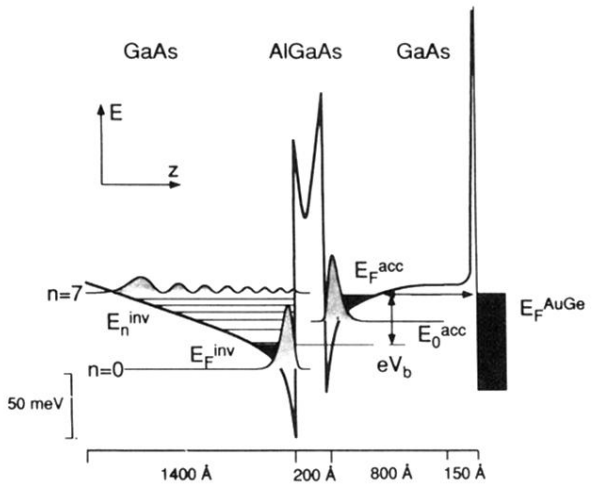

FIG. 1. Schematic view of the conduction-band profile at a bias voltage V_b. E_n^{inv} and E_0^{acc} denote the subband energies in the inversion and accumulation layers. E_F^{inv} and E_F^{acc} are the corresponding Fermi energies. E_F^{AuGe} is the Fermi energy in the top AuGe electrode and V_b is the applied bias voltage.